

SJÄLVSTÄNDIGA ARBETEN I MATEMATIK

MATEMATISKA INSTITUTIONEN, STOCKHOLMS UNIVERSITET

**Image super resolution,
an application of projection onto convex sets**

av

Martin Odenchrants

2018 - No M1

Image super resolution,
an application of projection onto convex sets

Martin Odencrants

Självständigt arbete i matematik 30 högskolepoäng, avancerad nivå

Handledare: Yishao Zhou

2018

Contents

1. Introduction.....	2
2. The image super resolution problem.....	4
3. Modeling image degradations.....	4
3.1. Formal problem definition	7
3.2. The Fredholm integral equation	8
3.3. Some mathematical concepts used in image processing.....	10
4. Review of earlier work on super resolution and the development of POCS.....	12
5. Projections onto convex sets.....	14
5.1. Convex sets and projections	15
5.2. Finding a common point in the intersection of convex sets by iteration	21
6. Finding projection operators	23
7. Image enhancement.....	27
7.1. Single image restoration by POCS	28
7.2. Image super resolution by POCS.....	30
8. Discussion and results	33

1. Introduction

Image resolution is a concept that most people are familiar with. A common interpretation of the term is how much detail that can be distinguished in an image, the higher detail the higher resolution. Even though high resolution images is something that we prefer to look at when looking at images of family or friends it's not always that a high resolution images can be registered. When an image is sampled below the resolution that is needed there are ways to increase the resolution. One way to increase the resolution in images is to rely on image super resolution (SR) techniques. SR is a theoretical framework used to obtain a high resolution (HR) image either from a single image or a sequence of low resolution images. HR images are needed in many applications and are mainly used either for improving the information in an image for human interpretation or for automatic machine perception [1]. There are several areas where image SR is of interest, these areas involve everything on the atomic to cosmic scale such as medical imaging, surveillance video, document processing and remote sensing to name a few. A well-known application familiar from TV is synthetic zooming for forensic purposes where a scene, for example a face is magnified in order to identify a criminal. Another example is tomographic images in medical applications where HR images can aid a doctor in the process of setting a correct diagnosis. A topic related to SR is single image restoration and it is from this field SR has evolved and several different approaches for solving the problem have been described in the literature. These approaches can be divided into two groups, mathematical and statistical and both spatial and frequency based solutions to the problem has been suggested. Early work on SR focused on solutions in the frequency domain but these techniques have shown to be difficult to apply in real world applications. Nowadays most work addresses the problem in the spatial domain the reason is its flexibility to handle a large variety of image degradations. Degradations refers to the various effects that degrades the resolution, these effects are always present when images are registered and can be divided into three groups, translation, blur and aliasing. For example, there is a loss of detail due to limited shutter speed, insufficient sensor density, noise within the sensor etc. Even though most people are familiar with the term resolution the term has different meaning in different contexts. In a SR context the term resolution refers to spatial resolution, the pixel spacing in an image and is usually measured in pixels per inch. The main restriction on the spatial resolution in an imaging system is the image sensor. Image sensors in digital cameras and smart phones are either a charged coupled device (CCD) or a complementary metal-oxide-semiconductor (CMOS) active-pixel sensor. A high number of sensor elements per unit area on the image sensor results in images with high spatial resolution. And imaging systems with a small number of sensor elements will capture images with low resolution with blocky effects due to aliasing from low sampling frequency. One straight forward solution to increase image resolution is to increase

the number of sensor elements per unit area and thus decreasing the size of each sensor element. But as the size of image sensor elements decreases the number of photons reaching each element will be low and as a result image quality will decrease due to enhancement of what is known as shot noise [2]. Other solutions connected to improved hardware have also been suggested but there is a high cost associated with high precision optics and sensors. Another more cost effective solution is to rely on SR techniques. In multiframe SR a sequence of low resolution images are registered onto a high resolution grid which is then used to estimate the final HR image. Mathematically the problem is formulated on the basis of the image observation model $g=Hf+e$, where g, H, f and e denote the observed image distribution, the degradation process, the actual image and the noise process respectively. Stated this way the recovery problem is an ill-posed inverse problem and there may not exist a unique solution and even if there is one, it may not depend continuously on data. The latter property of ill-posedness results in extreme sensitivity to observation noise. Regularization of an ill-posed problem refers to finding an acceptable estimate of an ideal solution that depends continuously on data. Two aspects of regularization are (i) quantitatively defining what an acceptable estimate is, and (ii) making use of a priori information on the components in the observation model [3]. The problem SR techniques tries to solve is to increase the spatial resolution given the limitations of a given imaging system. One method that makes use of a priori information is the method of projections onto convex sets (POCS). In 1967 Bregman published an article describing an iterative method for finding a vector located in an intersection of convex sets [4]. The method has since then been used in image recovery by several authors, among them Youla and Webb [5]. Conceptually the method can be described as follows, all known properties of an image X restricts X to lie in a well-defined convex set. If m properties of X can be defined, then X can be restricted to the intersection

$$C_0 = \bigcap_{i=1}^m C_i$$

of closed convex sets. With only the projection operators P_i on each closed convex C_i at hand, an estimate of X is found by a recursive scheme. The main synthesis of POCS is the realization of each C and P . Optimization, Fourier transforms, convex analysis, manifolds, non-expansive operators, fixed points etc. are all mathematical concepts connected to the POCS algorithm. SR with POCS is not a new area of research, the first application of POCS in image super resolution was published in the early 1980:s. Even so, looking at the mathematical concepts of POCS and the many different possible applications of SR results in an interesting opportunity to increase the author's mathematical skills in an area where there is clear connection between mathematical theory and application.

2. The image super resolution problem

A digital image is created by registering a continuous 2D signal of light intensities reflected from a natural scene. When any scene is captured with an imaging device there will be a difference between the original scene and the registered image. The difference between the two stems from several different sources related to the imaging device. Figure 1 illustrates the relationship between the scene that is to be captured and the image that is registered by the imaging device.

The input to the imaging system is a continuous scene that is approximated by band limited signals. These signals are altered by atmospheric noise before they reach the imaging device. Sampling the original signal at or beyond the Nyquist rate, a concept described in section 3, generates the HR image that corresponds to the original scene. In a super resolution setting there is usually some motion between the original scene and the imaging device, it is this movement that creates the sub pixel movements in the registered image sequence that makes SR possible. When the image signals move through the imaging device they get degraded by different blur effects. The blurred image is then down sampled at the imaging sensor when the signals are registered by the image sensor elements. The down sampled images are then again distorted by sensor noise and color filtering noise [1]. At the end the final version of the registered scene is a blurred, aliased and noisy version of the original scene.

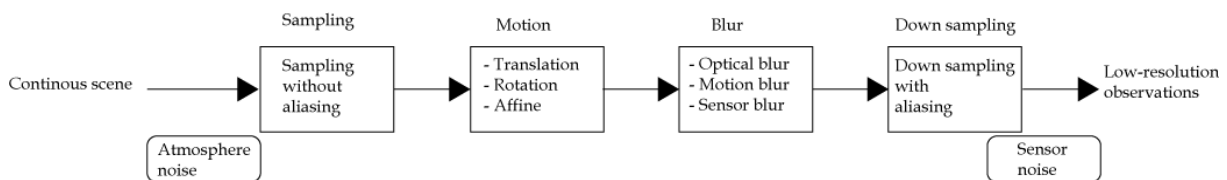


Figure 1: The various degradation effects present when registering an image

One solution to the problem of registering a HR image is to go for a very high resolution camera. In some situations this is not a viable option and SR techniques can be used in order to mitigate the degrading effects mentioned above. The problem one seeks to solve with multi frame SR techniques is to generate a HR image from a sequence of images representing the same scene.

3. Modeling image degradations

Several different effects contribute to the difference between the image registered by the imaging device and the actual scene. Blur is one of the more prominent effects and there is a lot of research available describing techniques for improving images that are degraded by blur. Overall, blur can be categorized into motion blur and out of focus blur. Out of focus blur can be considered as a spatial average of clear images by sampling the aperture. Motion blur can on the other hand be described as a temporal

average of clear images taken at different time instants by uniformly sampling the shutter period.

Images with motion blur can be created by registering images with a long exposure time. Exposure time is the time that the shutter is open and the sensor accumulates light from the objects in the scene. In the process of registering an image the diaphragm and the aperture statically limits the sensors exposure to light and the shutter limits the exposure to a finite range of time. During the time that the shutter is open several views of the moving object is registered since the sensor integrates all light hitting its surface. Motion blur is the result of interaction between light, diaphragm, aperture, sensor and the moving object. The effect is recognized by streaks in the image in the direction of motion. Movement of objects in the recorded scene and movement of the shutter are the two main reasons why motion blur appear in a scene. Motion blur due to movement of objects in the scene appear either due to motion of the imaging device relative to a static scene, movement of objects relative a static imaging device or due motion of both the imaging device and the scene.

Motion blur can be synthesized in images to make the images look more realistic, this can be accomplished in several different ways. Creating synthezised motion blur has been an active area of research since the late 1980s [8]. Linear space invariant motion blur can be synthesized with convolution of the registered image with a point spread function imitating motion of the imaging device relative a static scene. Out of focus blur can also be synthesized by convolution of the registered image with a point spread function imitating the specific out of focus blur effect.

Aliasing is an effect that occur when a continuous signal is under sampled, that is when the signal is discretely sampled at a rate that is insufficient to capture the changes in the signal. Under sampling results in images with artifacts that follow from high frequency components being folded into low frequency components. Consequently, image detail is lost since the high frequency components are not registered. More formally aliasing refers to the effect of sampling a bandlimited signal below the Nyquist rate. A function $f \in L_1(\mathbb{R})$ is said to be bandlimited if there exists $B \in \mathbb{R}$ such that $\text{sup}(\hat{f}) \subseteq [-B, B]$, here B is called a band limit for f and $\Omega := 2B$, is the corresponding frequency band and \hat{f} is the fourier transform of f . The Nyquist frequency of f is the minimal value of B such that $\text{sup}(\hat{f}) \subseteq [-B, B]$ and the corresponding frequency band is the Nyquist rate. In order to avoid aliasing the Shannon sampling theorem states that the signal needs to be sampled at twice the Nyquist frequency, when this criterion is met one can duplicate the original signal.

Theorem 3.1

If $f \in L_1(\mathbb{R})$ and \hat{f} , the Fourier transform of f , is supported on the interval $[-B, B]$, then

$$f(x) = \sum_{n \in \mathbb{Z}} f\left(\frac{n}{2B}\right) \text{sinc}\left(2B\left(x - \frac{n}{2B}\right)\right)$$

Where equality holds in the L_2 sense, that is, the series on the RHS of the equation converges to f in L_2 [11].

The word aliasing comes out of the fact that when a continuous signal is sampled below the Nyquist frequency the resulting discrete signal is just degraded copy of the original signal. Aliasing is an effect present in all applications where continuous signals are discretely sampled. To demonstrate the effect one can create a discrete sinusoid with normalized frequency according to

$$x[n] = x(nT_s) = A\cos(\omega nT_s + \theta) = A\cos(\hat{\omega}n + \theta)$$

In $\hat{\omega}$ represents the discrete time frequency which is also known as the principal alias, $\hat{\omega} = \omega T_s = \omega/f$, T represents the time between samples and f is the sampling rate. The continuous signal can be reconstructed if the principal alias of the discrete signal is scaled to the frequency of the continuous signal. As an example let the original 100 Hz signal that one want to reconstruct be on the following form $x(t) = \cos\left(2\pi(100)t + \frac{\pi}{3}\right)$, the corresponding Nyquist rate for this signal is then equal to 200 Hz. If one samples the signal at 0.4 times the Nyquist rate, $\hat{\omega} = 2.5$ and using this as the principal alias one will reconstruct a 20 Hz signal. The effect of aliasing in images is illustrated below, figure 2 shows a line of pixels in an image where there are two pixels in a cycle which is also the Nyquist frequency in this case. The bottom line in figure 2 illustrates the result when the image is sampled twice during each cycle, the result is a perfect replication of the original image.

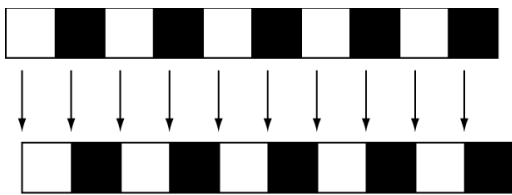


Figure 2: Effect of sampling the ideal signal at the Nyquist frequency

If the sampling rate is lowered to one sample in three pixels we get an indication of the result of down sampling a signal, this is illustrated in figure 3.

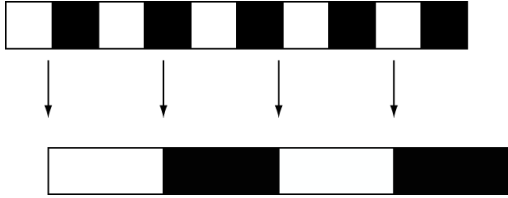


Figure 3: Effect of sampling the ideal signal below the Nyquist frequency

Looking at figure 3 we see that a new pattern emerges that is not present in the original image.

Super resolution has evolved from single restoration theory. As the name suggest single image restoration aims at improving an image from only one single image. This approach cannot be used to increase the image resolution by restoring the high frequency components that are hidden in the sampled signal. Super resolution theory on the other hand aims at restoring the high frequency components by using information contained in a sequence of images of the same scene and where the images differ by subpixel displacements.

3.1. Formal problem definition

The super resolution problem can be described as follows. Let $f(x_1, x_2, t), x_1, x_2, t \in \mathbb{R}$ denote the time-varying scene in the image plane coordinate system. Given a sequence of K low-resolution sampled images $y[m_1, m_2, k]$ with $m_1 \in \{1, 2, \dots, M_{1,k}\}, m_2 \in \{1, 2, \dots, M_{2,k}\}$ and $k \in \{1, 2, \dots, K\}$ acquired by imaging of the scene $f(x_1, x_2, t)$ at times $t_1 < t_2 < \dots < T$, here m_1, m_2 represents the vertical and horizontal pixels and k the number of acquired low-resolution images. The objective is to form S estimates $g[n_1, n_2, s], 1 \leq s \leq S$ of $f(x_1, x_2, t)$ on the discrete, super resolution sampling grid indexed by $[n_1, n_2]$ with $n_1 \in \{1, 2, \dots, N_{1,s}\}, n_2 \in \{1, 2, \dots, N_{2,s}\}$ at time instants $t_1 \leq \tau_1 < \tau_2 < \dots < \tau_S \leq T$. The individual estimates are the result of arbitrary geometric warping, linear space invariant blurring and uniform decimation on the ideal image $f(x_1, x_2, t)$. Furthermore each of the measured images is contaminated by additive Gaussian noise uncorrelated between estimates. The observed images g_k are related to f through the imaging model

$$g_k = D_k C_k F_k f + \varepsilon_k \text{ for } 1 \leq k \leq N$$

Where F_k is a $[N^2 \times N^2]$ matrix representing the geometric warp on f , C_k is the linear space variant blur matrix of size $[N^2 \times N^2]$ and D_k is a $[M^2 \times N^2]$ matrix representing the decimation of f_k .

Super-resolution refers to the reconstruction of images $g[n_1, n_2, s]$ that are visually superior to the original low resolution observations.

3.2. The Fredholm integral equation

The imaging model presented above is the matrix analogue to the Fredholm integral equations of the first kind. The following section describes the theory behind the problem to find a stable solution to the equation and is based on [15]. Fredholm integral equations appear in many applications, among them image processing, the Fredholm integral equation of the first kind has the following form.

$$g(x) = \int_a^b h(x, s)u(s)ds \quad c \leq x \leq d$$

In the above equation $g(x)$ represents the observed image, $h(x, s)$ represents the point spread function and $u(s)$ is the unknown function. The image recovery model presented above is an ill-posed inverse problem, there may not exist a unique solution and if a solution exists it may not depend continuously on the data. This last feature comes from the fact that small changes in g can result in very large changes in the solution. This property is not a result of using a particularly poor solution method but is inherent in the problem itself this can be understood by examining the underlying theory in more detail. In the following \mathcal{H} represents a Hilbert space, a normed linear vector space that is complete with respect to the defined norm.

Theorem 3.2. Let K be a linear operator from \mathcal{H}_1 to \mathcal{H}_2 . Then K is bounded if and only if it is continuous

If K is a bounded linear operator from \mathcal{H}_1 to \mathcal{H}_2 , its adjoint K^* is the bounded linear operator from \mathcal{H}_2 to \mathcal{H}_1 satisfying

$$(Ku, v) = (u, K^*v)$$

For all $u \in \mathcal{H}_1$ and $v \in \mathcal{H}_2$. If $K^* = K$, K is said to be self adjoint.

If $Ku = \lambda u$ for some nonzero $u \in \mathcal{H}$ and some number λ , λ is said to be an eigenvalue of K and u is the associated eigenvector. If K is self adjoint, the eigenvectors associated with the distinct eigenvalues are orthogonal. The domain $D(K)$ of K is that subset of \mathcal{H}_1 over which K is defined. The range $R(K)$ of K is defined by

$$R(K) = \{g: g = Ku \text{ for some } u \in D(K)\}$$

And the null space $N(K)$ of K is defined by

$$N(K) = \{u: Ku = 0\}$$

A linear operator K mapping \mathcal{H}_1 to \mathcal{H}_2 is called compact if $\overline{K(B)}$ is compact for every bounded subset B of \mathcal{H}_1 .

Theorem 3.3. Let K be a compact self-adjoint operator from the Hilbert space \mathcal{H} into itself. Then for each nonzero eigenvalue λ of K the set $N(K - \lambda I)$ is finite-dimensional. The eigenvalues $\lambda_1, \lambda_2, \dots$ form a sequence that converges to zero unless their number is finite.

Theorem 3.4. Let K be a compact self adjoint linear operator with eigenvalues $\lambda_1, \lambda_2, \dots$ repeated according to the dimension of the associated space $N(K - \lambda I)$. Let u_1, u_2, \dots be the corresponding orthonormal eigenvectors. Then for any $u \in \mathcal{H}$

$$Ku = \sum_{n=1}^{\infty} \lambda_n (u, u_n) u_n$$

If K has only a finite number of eigenvalues, the sum above will be finite and K is said to have finite rank and $R(K)$ is a finite dimensional set.

Now let K be a compact linear operator from \mathcal{H}_1 to \mathcal{H}_2 , then K^*K is a compact self adjoint linear operator mapping \mathcal{H}_1 to itself. The eigenvalues of K^*K are all nonnegative and listed in a decreasing sequence they are $\lambda_1 \geq \lambda_2 \geq \dots \geq 0$. Let v_1, v_2 be a corresponding sequence of orthonormal eigenvectors of K^*K and set

$$\mu_n = 1/\sqrt{\lambda_n}$$

and

$$u_n = \mu_n K v_n$$

Then $\{u_n\}$ is orthonormal sequence in \mathcal{H}_2 satisfying

$$\mu_n K^* u_n = v_n$$

Theorem 3.5. $\{u_n\}$ is an orthonormal basis for $\overline{R(K)} = [N(K^*)]^\perp$ and $\{v_n\}$ is an orthonormal basis for $\overline{R(K^*)} = [N(K)]^\perp$. The sequence of triples $\{u_n, v_n; \mu_n\}$ is called a singular system for K . It follows from $\mu_n = 1/\sqrt{\lambda_n}$ that the singular values μ_n become arbitrarily large as n increases unless K is finite dimensional.

Theorem 3.5. Let K be a compact linear operator mapping \mathcal{H}_1 to \mathcal{H}_2 , and let $\{u_n, v_n; \mu_n\}$ be a singular system for K . The equation $Ku = g$ has a solution if and only if the following conditions hold

- i. $g \in [N(K^*)]^\perp$.
- ii. $\sum_{n=1}^{\infty} \mu_n^2 |g, u_n|^2 < \infty$

When these conditions are met, the solution is given by

$$u = \sum_{n=1}^{\infty} \mu_n(g, u_n) v_n$$

The above theorem indicates the effect of small changes in observed data on the solutions to the Fredholm equation. The sequence of inner products (g, u_n) must decrease rapidly enough to counter the increase in the singular values μ_n , if the above equation is used to solve the Fredholm equation the singular values will increase as n increases and small perturbations in the higher modes will result in large changes in the solution.

A consequence of the inherent difficulties to obtain a stable solution to the above problem has been different techniques for overriding the increasing effect of the singular values as n gets large. These techniques are referred to as regularization in the literature and one well known regularization technique is Tikhonov regularization. One way of using Tikhonov regularization is in combination with total least squares, another regularization technique is POCS.

3.3. Some mathematical concepts used in image processing

Convolution is an operation that can be used in image processing in order to synthesize degradation of the original scene with different blur effects. The original scene is convolved with a point spread function to create the observed image. When the convolution of the observed image and the point spread function is assumed to be circular, the derivation of some projection operators is simplified.

The circular convolution between a given signal $f(n)$ and point spread function $h(n)$ is defined as

$$g(n) = f(n) \circledast h(n) = \sum_{m=0}^{N-1} f(m)h(n - m)$$

The convolution between a given signal and a point spread function can also be described with a Toeplitz matrix. A Toeplitz matrix is an $n \times n$ matrix $T_n = [t_{k,j}; k, j = 0, 1, \dots, n-1]$ where $t_{k,j} = t_{k-j}$ and is constructed as follows

$$T_n = \begin{bmatrix} t_0 & t_{-1} & t_{-2} & \dots & t_{-(n-1)} \\ t_1 & t_0 & t_{-1} & & \\ t_2 & t_1 & t_0 & & \\ \vdots & & & & \\ t_{n-1} & & & \dots & t_0 \end{bmatrix}$$

When every row of the matrix is a right cyclic shift of the row above it $t_k = t_{k-n}$ for $k = 1, 2, \dots, n-1$ the matrix is said to be circulant and is on the following form

$$C_n = \begin{bmatrix} t_0 & t_{-1} & t_{-2} & \dots & t_{-(n-1)} \\ t_{-(n-1)} & t_0 & t_{-1} & & \\ t_{-(n-2)} & t_{-(n-2)} & t_0 & & \\ \vdots & & & & \\ t_{-1} & t_{-2} & & \dots & t_0 \end{bmatrix}$$

Circulant matrices appear in applications involving the discrete Fourier transform. Fourier transforms is another concept that has several applications in image processing. Fourier transforms can be used to define convex sets based on the spectral properties of the target image that can be used in the POCS algorithm. Another use of Fourier transforms in image processing is to translate the convolution of two signals to multiplication of Fourier coefficients. Since multiplication of the Fourier coefficients is equal to circular convolution, the Fourier transform is an effective way to convolve an image with a point spread function. The close connection between circular convolution and multiplication of Fourier coefficients can be seen below.

First let the discrete Fourier transform of $f(n)$ be defined as

$$F(k) = \sum_{n=0}^{N-1} f(n) e^{-j\frac{2\pi}{N}kn}$$

And the inverse transform be defined as

$$f(n) = \frac{1}{N} \sum_{k=0}^{N-1} F(k) e^{j\frac{2\pi}{N}kn}$$

Then

$$g(n) = \frac{1}{N} \sum_{k=0}^{N-1} F(k) H(k) e^{j\frac{2\pi}{N}kn}$$

$$\begin{aligned} g(n) &= \frac{1}{N} \sum_{k=0}^{N-1} \sum_{m=0}^{N-1} f(m) e^{-j\frac{2\pi}{N}km} H(k) e^{j\frac{2\pi}{N}kn} \\ &= \sum_{m=0}^{N-1} f(m) \left(\frac{1}{N} \sum_{k=0}^{N-1} H(k) e^{j\frac{2\pi}{N}k(n-m)} \right) \end{aligned}$$

And since $\left(\frac{1}{N} \sum_{k=0}^{N-1} H(k) e^{j\frac{2\pi}{N}k(n-m)} \right) = h(n-m)$ it is found that

$$g(n) = \sum_{m=0}^{N-1} f(m) h(n-m)$$

It was mentioned above that the derivation of projection operators can be simplified when the convolution is circular, this follows from a result connected to Plancharel's theorem. With the aid from Plancharel's theorem one can find the norm of a signal from its Fourier coefficients. Let the signal $f(n)$ be described by a vector with elements U_n then

$$\begin{aligned} \|U\|^2 &= \langle U, U \rangle = \left\langle \left(\frac{1}{N} \sum_{n=0}^{N-1} \widehat{U}_n e^{j2\pi nk/N} \right), \left(\frac{1}{N} \sum_{m=0}^{N-1} \widehat{U}_m e^{j2\pi mk/N} \right) \right\rangle \\ &= \frac{1}{N^2} \sum_{n=0}^{N-1} \sum_{m=0}^{N-1} \langle \widehat{U}_n e_n \rangle \langle \widehat{U}_m e_m \rangle = \frac{1}{N^2} \sum_{n=0}^{N-1} \sum_{m=0}^{N-1} \widehat{U}_n \widehat{U}_m \langle e_n, e_m \rangle \\ &= \frac{1}{N^2} \sum_{n=0}^{N-1} \widehat{U}_n \widehat{U}_n N = \frac{1}{N} \sum_{n=0}^{N-1} |\widehat{U}_n|^2 \end{aligned}$$

In the second to last line e_n has been used to represent the vector $e^{j2\pi nk/N}$ and since $\langle e_n, e_m \rangle = 0$ and $\langle e_n, e_n \rangle = 1$, the result follows.

4. Review of earlier work on super resolution and the development of POCS

Super resolution stems from single image restoration theory and there is a clear connection between two problems. The earliest work on super resolution can be traced back to the 1980:s when Tsay and Huang worked on improving the resolution of

Landsat images. Landsat records images of the same areas of the earth during orbits and thus produces a sequence of similar but not identical images. The acquired images are treated as aliased images, of a static scene undergoing translational motion. As mentioned above recorded images are degraded versions of the scene they represent, the degradation is due to aliasing, motion, blur and noise. Tsay and Huang propose a frequency based solution to the problem based on the shift and aliasing properties of the continuous Fourier transform. The shift and aliasing properties are used to formulate a system of equations that relate the discrete fourier transform coefficients of the observed images to samples of the continuous fourier transform of the original unknown scene which is recovered using the inverse discrete fourier transform. In order to solve the system of equations, data on the translational motion is needed. With this information the method is a computationally efficient to use. However there are several drawbacks with the proposed method, for example there is no room for modeling a point spread blur function and the effect of noise is not considered. Tekalp, Ozkan and Sezan [6] identified these problems and proposed an alternative that gives the possibility to model a space invariant point spread function with noise. Similar to Tsay and Huang a frequency based approach is used and the final super resolution image is obtained by solving a system of equations similar to Tsay and Huang. Several other authors have contributed with work on super resolution in the frequency domain, even though there are advantages there are also disadvantages that the frequency based methods have a difficulty to handle. A fundamental problem with the frequency based methods is the assumption of global motion, this assumption is difficult to motivate in most real world applications. Yet another disadvantage is that there is no possibility to consider a priori information in order to regularize the solution [15]. A regularization approach is usually an attractive alternative due to the ill posed nature of the super resolution problem.

Several authors have contributed with suggestions on how to solve the SR problem with POCS. An early example is an article from Oskoui and Stark [7] who worked on restoring images in computerized tomography. In their work they show that there is a connection between POCS and algebraic reconstruction technique (ART). They discuss differences and similarities between the two methods and one of the results is that ART can be viewed as a primitive version of POCS and that images restored with ART can be improved with the use of a priori constraints. However in a situation where a relatively complete data set is available, the use of a priori constraints will have little influence ART reconstruction. The strength of POCS arises when the available data set is not complete, exploiting known constraints results in a solution that is superior to plain ART reconstruction. Similar to the development of the frequency based SR methods there a number of super resolution problems where variations of POCS have been suggested with the aim to handle more complicated degradations. In [8] Oskoui and Stark continue their work on improving image resolution in CT. One difference is

that reconstruction in their previous contribution is based on a set of line integrals while the work in the new article aims at reconstruction with the aid of a set of area integrals.

Image blur can be categorized into two groups, linear space invariant (LSI) and linear space variant (LSV). Most work encountered in the literature treats the LSI case, nevertheless in real world applications, the degradations are often space varying. Two examples of LSV blur is when an image contains an accelerating object or when an image contains out of focus blur, which can be the case when a scene has depth. Even though most SR work treats the LSI case there are examples where the LSV case has been studied. Several approaches have been considered, a few examples are sectional methods, Kalman filtering and POCS. An example where space varying blur is treated with POCS can be found in [9]. The constraint set considered is similar to what was used in [8], a bounding residual constraint. In order to treat LSV blur the PSF needs to be estimated in a first step. With the estimated PSF the constraint sets can be defined. In [9] Tekalp and Sezan compares the LSV POCS approach with an alternative method, ROMKF and discusses two factors that have an impact on the final solution, the a priori bound on the residual and the number of iterations. In conclusion the space varying POCS approach is shown to be computationally efficient and is also robust to errors in the point spread estimation.

5. Projections onto convex sets

Noise and blur are the main sources of image degradation. In the early days of super resolution these effects were modeled as if they were global. In many real world applications this assumption does not hold. Motion for example is an effect that is usually local within an image, one example is a moving car. Set theoretic methods where POCS is one example are well suited for degradations that are local. When there is information available on or a possibility to estimate degradations POCS incorporates the information by formulating constraint sets accordingly. Constraint sets are defined as convex sets in $\mathcal{H}^{N_1 \times N_2}$, these sets represents all possible reconstructions of the original scene. A number of different constraint sets can be formulated, examples are positivity, bounded energy, smoothness etc. The solution to the super resolution problem with POCS is any image in the intersection of the defined constraint sets. A solution to the super resolution problem with POCS is found by projecting an initial estimate of the solution on the constraint sets in a sequential manner until a point in the intersection is found. Given k convex constraint sets in $\mathcal{H}^{N_1 \times N_2}$ such that the intersection of the sets is non-empty, POCS projects a point onto each constraint set, repeating until a point is reached which is in the intersection of the k sets. It can be shown that provided the constraint sets are convex that this iteration converges. The following sections are based on [12] and [13].

5.1. Convex sets and projections

Defintion 5.1. A subset C of \mathbb{R}^n is called convex if

$$\alpha x + (1 - \alpha)y \in C \quad \forall x, y \in C, \forall \alpha \in [0, 1]$$

According to the definition a set is convex if the line segment connecting two elements of the set is contained within the set.

Definition 5.2. The epigraph of a function $f: X \rightarrow [-\infty, \infty]$ where $X \subset \mathbb{R}^n$ is the subset of \mathbb{R}^{n+1} given by

$$\text{epi}(f) = \{(x, w) \mid x \in X, w \in \mathbb{R}, f(x) \leq w\}$$

Theorem 5.1. Let $X \subset \mathbb{R}^n$ and let $f: X \rightarrow \mathbb{R}$, then the epigraph of f is a convex set if f is convex.

Proof. Since f is assumed to be convex one can choose $(x_1, y_1) \in \text{epi}(f)$ and $(x_2, y_2) \in \text{epi}(f)$ and $0 < \lambda < 1$ it follows then

$$\lambda y_1 + (1 - \lambda)y_2 \geq \lambda f(x_1) + (1 - \lambda)f(x_2) \geq f(\lambda x_1 + \lambda x_2)$$

therefore $\lambda(x_1, y_1) + (1 - \lambda)(x_2, y_2) \in \text{epi}(f)$.

Example 5.1. A disc with radius r is convex. Let the disc, D , be centered at the origin $D = \{x \mid \|x\|^2 \leq r^2\}$ and let $0 \leq \lambda \leq 1$. Let u and v belong to the disk. And let $z = \lambda u + (1 - \lambda)v$. Then

$$\|z\| = \|\lambda u + (1 - \lambda)v\| \leq \lambda\|u\| + (1 - \lambda)\|v\| \leq \lambda r + (1 - \lambda)r = r$$

And z is contained within the disk.

The illustration below gives an example of a convex and nonconvex set.

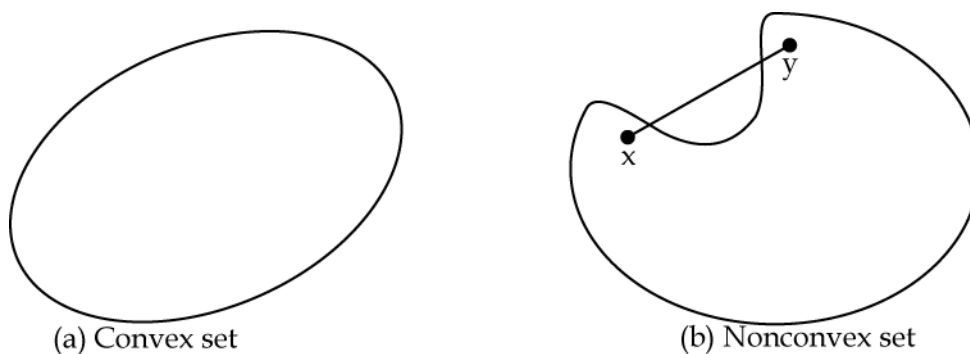


Figure 4: Illustration of convex and nonconvex set.

Proposition 5.1. The intersection $\bigcap_{i \in I} C_i$ of any collection $\{C_i \mid i \in I\}$ of convex sets is convex.

As a consequence, the intersection of two disks is a convex set. If D_1 and D_2 are two disks with intersection $D_1 \cap D_2$ and $u, v \in D_1 \cap D_2$. Then, $z \in D_1$ and $z \in D_2$ where $z = \lambda u + (1 - \lambda)v$.

Definition 5.2. Given an arbitrary set C in \mathbb{R}^n . The convex hull of C , denoted $\text{conv}(C)$, is the collection of all convex combinations of C . This means that $\text{conv}(C) = \{y = \sum_{i=1}^k \lambda_i y_i \mid y_i \in C, \sum_{i=1}^k \lambda_i = 1, \lambda_i \geq 0\}$

Definition 5.3. A set $C \subseteq \mathcal{H}$ is closed if and only if every convergent sequence in \mathcal{H} is completely contained in C has its limit in C .

A set that is both convex and closed is called a closed convex set.

One property of closed and convex sets, that is central to the POCS method, is that of a closest point. Given a point $x \notin C$ there is a unique point $\bar{y} \in C$ with minimum distance from x and a hyperplane that separates x and C such that

$$\inf_{y \in C} \|x - y\| = \|x - \bar{y}\|$$

Theorem 5.1. Let C be a closed convex set in \mathbb{R}^n and $x \notin C$. Then there exists a unique point $\bar{y} \in C$ with minimum distance from x . Furthermore, y is the minimizing point if and only if $\langle x - \bar{y} \rangle^t \langle y - \bar{y} \rangle \leq 0$ for all $y \in C$.

Theorem 5.1 leads to the concept of a projection operator. For any $x \in \mathcal{H}$ the projection $P_C x$ of x onto C is the element in C with closest distance to y .

$$\|x - P_C x\| = \min_{y \in C} \|x - y\|$$

The projection operator projecting onto a closed convex set in a Hilbert space maps a point outside the set onto the closest, unique, point in the set.

Corollary 5.1. If some $z \in C$ has the property

$$\langle x - z \rangle^t \langle y - z \rangle \leq 0$$

for all $y \in C$, then $z = P_C x$.

The fact that $\langle x - P_C x \rangle^t \langle y - P_C x \rangle \leq 0$ means that the vector $x - P_C x$ is supporting C at $P_C x$, this is illustrated in figure 5. In figure 5 one can see that the angle between $x - P_C x$ and $y - P_C x$ for any point in C is greater or equal to 90° . C can be seen to lie in the halfspace $\alpha^t \langle y - P_C x \rangle \leq 0$ relative to the hyperplane $\alpha^t \langle y - P_C x \rangle = 0$ passing through $P_C x$ and having normal $\alpha = x - P_C x$.

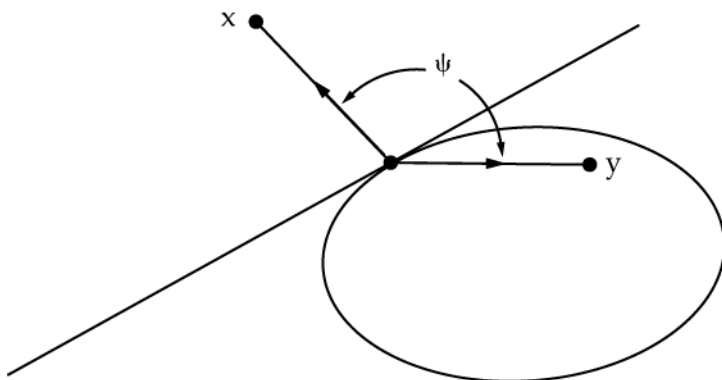


Figure 5: Support of the convex set C .

Theorem 5.2. Let C be any closed convex set. Then for any pair of elements x and y in \mathcal{H} ,

$$\|P_C x - P_C y\|^2 \leq \langle x - y \rangle^t \langle P_C x - P_C y \rangle$$

Corollary 5.2. Projection operators onto closed convex sets are nonexpansive and therefore continuous.

Proof. By applying Schwarz to the above expression, yields for any x and y in \mathcal{H}

$$\|P_C x - P_C y\|^2 \leq \langle x - y \rangle^t \langle P_C x - P_C y \rangle \leq \|P_C x - P_C y\| \|x - y\|$$

Under the projection P_C , the distance between the two images never exceeds the distance between the two original points. If the distance $\|x - y\|$ is small $\|P_C x - P_C y\|$ is small and P_C is continuous.

Definition 5.4. A mapping $T: C \rightarrow \mathcal{H}$ is said to be a contraction if there exists a positive constant, $0 < \theta < 1$, such that

$$\|Tx - Ty\| \leq \theta \|x - y\|$$

for all $x, y \in C$

A point $x \in \mathcal{H}$ is said to be a fixed point of a mapping T if $Tx_1 = x_1$

Any contraction has at most one fix point. If $Tx_1 = x_1$ and $Tx_2 = x_2$ then

$$\|x_1 - x_2\| = \|Tx_1 - Tx_2\| \leq \theta \|x_1 - x_2\|$$

Therefore $\|x_1 - x_2\| = 0$ and $x_1 = x_2$

Theorem 5.4. If C is a nonempty closed subset of \mathcal{H} , any contraction mapping T of C into itself possesses a unique fix point x_∞ . Starting from any element x_0 of C , $T^n x_0 \rightarrow x_\infty$ as $n \rightarrow \infty$

Since contraction is difficult to achieve in many applications the method of POCS relies on the following weaker concept.

Definition 5.5. A mapping $T: C \rightarrow \mathcal{H}$ is said to be nonexpansive if

$$\|Tx - Ty\| \leq \|x - y\|$$

For all $x, y \in C$

Properties of nonexpansive- and asymptotic regular operators plays a key role in the convergency theory of POCS, these properties are presented below.

Theorem 5.5. Let $T: C \rightarrow C$ be a nonexpansive map whose domain C is a nonempty closed bounded convex set. Then T has at least one fixed point.

Proof. Let y_0 be any preselected member of C and let the set $C_0 = \{x | x = y - y_0, y \in C\}$. The translate C_0 is also a closed bounded set which also contains the zero vector ϕ . Every $x \in C_0$ possesses a unique decomposition $x = y - y_0, y \in C$. Let $F: C_0 \rightarrow C_0$ be defined by

$$Fx = Ty - y_0$$

this map F is nonexpansive since $x_1 = y_1 - y_0$ and $x_2 = y_2 - y_0$ imply that

$$\|Fx_1 - Fx_2\| = \|Tx_1 - Tx_2\| \leq \|y_1 - y_2\| = \|(y_1 - y_0) - (y_2 - y_0)\| = \|x_1 - x_2\|$$

For any fixed $k, 0 < k < 1$, the map $G = kF$ is a contraction of C_0 into itself. For any $x \in C_0, kFx = k(Fx) + (1 - k)\phi \in C_0$ and for all $x_1, x_2 \in C_0$

$\|Gx_1 - Gx_2\| = k\|Fx_1 - Fx_2\| \leq k\|x_1 - x_2\|$ according to theorem 5.4 there exists a unique $x_k \in C_0$ for every $k, 0 < k < 1$ such that

$$x_k = kFx_k$$

the next step is to show that if $x_k \rightarrow g$ as $k \rightarrow 1$ from below, then by the continuity of F and $g \in C_0$ it follows that $g = Fg$. This is accomplished if it can be proved that

$$\lim_{k \rightarrow 1, 0 < k < 1} x_k = g$$

where g is the unique fixed point of F in C_0 of minimum norm. Assume that $0 < k < l \leq 1, x_k = kFx_k, x_l = lFx_l$ and let $h = x_l - x_k$. Then, since $\|Fx_l - Fx_k\| \leq \|x_l - x_k\|$ it follows that

$$\langle l^{-1}(x_k + h) - k^{-1}x_k, l^{-1}(x_k + h) - k^{-1}x_k \rangle \leq \|h\|^2$$

and also

$$(l^{-1} - k^{-1})^2 \|x_k\|^2 + (l^{-2} - 1) \|h\|^2 \leq 2l(k^{-1} - l^{-1}) \text{Re}\langle x_k, h \rangle$$

and it follows that

$$\text{Re}\langle x_k, h \rangle \geq 0$$

which combined with the identity

$$\|x_l\|^2 = \|x_k + h\|^2 = \|x_k\|^2 + \|x_l\|^2 + 2\text{Re}\langle x_k, h \rangle$$

gives the following inequality

$$\|x_l\|^2 \geq \|x_k\|^2 + \|x_l - x_k\|^2$$

for any choice of sequence $0 < k_1 < k_2 < \dots$ such that $k_i \rightarrow 1$, the sequence $\{\|x_{k_i}\|\}$ is monotone and nondecreasing and bounded. It therefore converges, and

$$\|x_l - x_k\|^2 \leq \|x_l\|^2 - \|x_k\|^2 \rightarrow 0$$

As $l, k \rightarrow \infty$. By the completeness of $\mathcal{H}, x_{k_i} \rightarrow g \in C_0$ since C_0 is closed.

To finish up, let e be any fixed point of F in C_0 . Then $e = 1 \cdot Fe$ and it possible to apply $\|x_l\|^2 \geq \|x_k\|^2 + \|x_l - x_k\|^2$ with $x_l = e, l = 1, x_k = x_{k_i}$, and $k = k_i$ for any $i = 1 \rightarrow \infty$. As $i \rightarrow \infty, x_{k_i} \rightarrow g$, and

$$\|e\|^2 \geq \|g\|^2 + \|e - g\|^2 \geq \|g\|^2$$

Therefore, $\|g\| = \inf\|e\|$, as e ranges over the fixed points of F in C_0

Theorem 5.5 rests on the assumptions of boundedness and convexity. This assumption can usually not met in applications because numerical bounds are not always available. But if the existence of a fixed point is known in advance, the boundedness requirement can be dropped. In order to reach a first theorem on convergence of successive projections to a fixed point three lemmas are needed.

Lemma 5.1. The set of fixed points \mathfrak{F} of a nonexpansive mapping T with closed convex domain C and range \mathcal{H} is a closed convex set.

Proof. Let $x_i = Tx_i, i = 1 \rightarrow \infty$, and suppose that $x_i \rightarrow x$. Since $\{x_i\} \subset C$ which is closed, $x \in C$ and Tx is well defined, invoking nonexpansivity,

$$\|Tx - x\| = \|Tx - Tx_i + x - x_i\| \leq 2\|x - x_i\| \rightarrow 0$$

Therefore \mathfrak{F} is closed. To establish convexity the following identity is used.

$$\|x - y\|^2 - \|Tx - Ty\|^2 = 4\operatorname{Re}\langle Px - Py, (1 - P)x - (1 - P)y \rangle$$

Where $P = (1 + T)/2$

Since T is nonexpansive

$$\operatorname{Re}\langle Px - Py, (1 - P)x - (1 - P)y \rangle \geq 0$$

For every $x, y \in C$. Since P and T have the same fixed point it suffices to show that the set of fixed points of P is convex. Let y be any fixed point of P then the above equation reduces to $\operatorname{Re}\langle Px - y, x - Px \rangle \geq 0$

For all $x \in C$. Conversely, if some $y \in C$ satisfies $\operatorname{Re}\langle Px - y, x - Px \rangle \geq 0$ for every $x \in C$ it satisfies it for $x = y$, which indicates that $\|y - Py\| \leq 0$ or $y = Py$. The set of fixed points of T is therefore the set of all $y \in C$ that satisfies $\operatorname{Re}\langle Px - y, x - Px \rangle \geq 0$ for all $x \in C$, and this set is convex.

Definition 5.6. A map $T: C \rightarrow \mathcal{H}$ is said to be demiclosed if it from

$$\{x_n\} \subset C, \{x_n\} \rightarrow x_0, x_0 \in C, Tx_n \rightarrow y_0$$

in the above definition the symbols \rightarrow, \rightarrow represents weak and strong convergence respectively and it follows that $Tx_0 = y_0$

Definition 5.7. A map $T: C \rightarrow C$ is said to be asymptotically regular if for every $x \in C, T^n x - T^{n+1} x \rightarrow \phi$

Lemma 5.2. In a Hilbert space \mathcal{H} let the sequence $\{x_n\}$ converge weakly to x_0 . Then, for any $x \neq x_0$,

$$\lim_{n \rightarrow \infty} \inf \|x_n - x\| > \lim_{n \rightarrow \infty} \inf \|x_n - x_0\|$$

Lemma 5.3. Let T be any nonexpansive map with closed convex domain $C \subset \mathcal{H}$ then $1 - T$ is demiclosed

Proof. Let $\{x_n\} \subset C$ converge weakly to x_0 and let $\{x_n - Tx_n\}$ converge strongly to y_0 . Then, since T is nonexpansive

$$\begin{aligned} \liminf_{n \rightarrow \infty} \|x_n - x_0\| &\geq \liminf_{n \rightarrow \infty} \|Tx_n - Tx_0\| \\ &= \liminf_{n \rightarrow \infty} \|Tx_n - x_n + x_n - Tx_0\| = \liminf_{n \rightarrow \infty} \|x_n - y_0 - Tx_0\| \geq \liminf_{n \rightarrow \infty} \|x_n - x_0\| \end{aligned}$$

by lemma 5.2. And by again by lemma 5.2 $x_0 = y_0 - Tx_0$ or $(1 - T)x_0 = y_0$ so $1 - T$ is demiclosed.

Theorem 5.6. Let $T: C \rightarrow C$ be an asymptotically regular nonexpansive map with closed convex domain $C \subset \mathcal{H}$ whose set of fixed points $\mathfrak{F} \subset C$ is nonempty. Then, for any $x \in C$, the sequence $\{T^n x\}$ is weakly convergent to an element of \mathfrak{F}

Proof. See appendix A

Corollary. The sequence $\{T^n x\}$ converges strongly to y_0 iff at least one of its subsequences converges strongly.

Definition 5.8. Given a mapping $T: C \rightarrow C$ the corresponding relaxed operator is defined as the convex combination

$$T_\alpha = \alpha I + (1 - \alpha)T$$

Where I denotes the identity operator and α is an arbitrary nonnegative real number.

Definition 5.9. A mapping $C \rightarrow C$ is said to be a reasonable wanderer if for every $x \in C$

$$\sum_{n=0}^{\infty} \|T^n x - T^{n+1} x\|^2 < \infty$$

Theorem 5.7. Let $T: C \rightarrow C$ be a nonexpansive mapping with closed convex domain C whose set of fixed points is nonempty. Then for any fixed α , $0 < \alpha < 1$, $T_\alpha: C \rightarrow C$ is reasonable wanderer and the sequence $\{T_\alpha^n x\}$ converges weakly to a fixed point of T for every $x \in C$.

In the above theorem the assumption of asymptotic regularity of the mapping, which was a part of theorem 5.6, is dropped. And it is shown that weak convergence can be reached if the mapping is a reasonable wanderer. An example of a nonexpansive operator that is not asymptotically regular can be constructed as $Tx = -x$. T is nonexpansive and maps C into C and the only fix point of T is $x = 0$. But T is not asymptotically regular since $T^n x - T^{n+1} x = 2(-1)^n x \not\rightarrow 0$ as $n \rightarrow \infty$. Even so the convex combination

$$T_\alpha = \alpha I + (1 - \alpha)T$$

Is a reasonable wanderer for all α in the interval $0 < \alpha < 1$.

5.2. Finding a common point in the intersection of convex sets by iteration

In the image recovery problem to be solved, every known property of the original image x restricts x to lie in a closed convex subset of \mathcal{H} . Restrictions regarding the properties of x , e.g. the deviation of x from a reference image etc, can be used to construct a subset of \mathcal{H} , therefore if m restrictions can be defined x will be contained in the intersection of these sets,

$$x \in C_0 = \bigcap_{i=1}^m C_i$$

Since each C_i is closed and convex C_0 is closed and convex. If the operator projecting the observed image on C_0 is known the problem is solved, $P_0x \in C_0$. However, since C_0 is based on the intersection of m closed convex subsets, the structure of C_0 can be considerably more complex than each C_i . As a consequence a realization of P_0 may not be possible. Since projection operators on convex sets are nonexpansive and therefore possess at least one fix point, each P_i has at least one fix point. The fix points of P_i is also a fix point of P_0 and also a fix point of the composition

$$T = P_m P_{m-1} \dots P_1$$

And more generally

$$T = T_m T_{m-1} \dots T_1$$

Where $T_i = 1 + \lambda_i(P_i - 1)$. The key question of POCS is if the converse also holds, are the fix points of T contained in C_0 and if so, does the sequence $\{T^n x\}$ converge weakly or strongly, and what are the effect of the initialization point. The first theorem below addresses the question of weak convergence.

Theorem 5.8. Let C_0 be nonempty. Then, for every $x \in \mathcal{H}$ and every choice of constants $\lambda_1, \lambda_2, \dots, \lambda_m$ in the interval $0 < \lambda < 2$, the sequence $\{T^n x\}$ converges weakly to a point of C_0 .

Proof. For $0 < \lambda_i < 2$ T is nonexpansive, the assertion is true for $0 \leq \lambda_i \leq 1$ since

$$\begin{aligned} \|T_i x - T_i y\| &= \|(1 + \lambda(P_i - 1))x - (1 + \lambda(P_i - 1))y\| \\ &= \|(1 - \lambda)(x - y) + \lambda P_i(x - y)\| \end{aligned}$$

$$\leq (1 - \lambda)\|x - y\| + \lambda\|x - y\|$$

And for $1 < \lambda_i$

$$\begin{aligned} \|T_i x - T_i y\|^2 &= \|(1 - \lambda_i)(x - y) + \lambda_i P_i(x - y)\|^2 \\ &= (1 - \lambda_i)^2 \|x - y\|^2 + 2\lambda_i(1 - \lambda_i) \operatorname{Re}\langle x - y, P_i x - P_i y \rangle + \lambda_i^2 \|P_i x - P_i y\|^2 \\ &\leq (1 - \lambda_i)^2 \|x - y\|^2 + (\lambda_i^2 + 2\lambda_i(1 - \lambda_i)) \|P_i x - P_i y\|^2 \end{aligned}$$

$$\begin{aligned} \text{since } \|P_i x - P_i y\|^2 &\leq \operatorname{Re}\langle x - y, P_i x - P_i y \rangle \\ &= (1 - \lambda_i)^2 \|x - y\|^2 + \lambda_i(2 - \lambda_i) \|P_i x - P_i y\|^2 \\ &\leq (\lambda_i(2 - \lambda_i) + (1 - \lambda_i)^2) \|x - y\|^2 = \|x - y\|^2 \end{aligned}$$

And T is nonexpansive.

For the sequence $\{T^n x\}$ to converge to a fix point, the next step is to show that T is a reasonable wanderer for $0 < \lambda < 2$ and convex sets $i = 1, \dots, m$.

For $m = 1$ $T = T^1$, $C_0 = C_1$, and

$$\|x - Tx\|^2 = \lambda^2 \|P_1 x - x\|^2$$

And also

$$\begin{aligned} \|Tx - y\|^2 &= \|x - y + \lambda_1(P_1 x - x)\|^2 \\ &= \|x - y\|^2 + 2\lambda_1 \operatorname{Re}\langle x - y, P_1 x - x \rangle + \lambda_1^2 \|x - P_1 x\|^2 \\ &= \|x - y\|^2 + \lambda_1(2 - \lambda_1) \|x - P_1 x\|^2 + 2\lambda_1 \operatorname{Re}\langle x - P_1 x, y - P_1 x \rangle \\ &\leq \|x - y\|^2 - \lambda_1(2 - \lambda_1) \|x - P_1 x\|^2 \end{aligned}$$

Follows since the last term in the second to last expression above is nonpositive. By combination of $\|x - Tx\|^2 = \lambda^2 \|P_1 x - x\|^2$ and $\|x - y\|^2 - \lambda_1(2 - \lambda_1) \|x - P_1 x\|^2$ the expression below follows

$$\|x - Tx\|^2 \leq \frac{\lambda_1}{2 - \lambda_1} (\|x - y\|^2 - \|Tx - y\|^2)$$

For $m \geq 1$ induction over m gives the inequality

$$\|x - Tx\|^2 \leq b_m \cdot 2^{m-1} (\|x - y\|^2 - \|Tx - y\|^2)$$

Let $T = T_m K$, where $K = T_{m-1} T_{m-2} \dots T_1$

Then for $m \geq 2$

$$\|x - Tx\|^2 \leq 2(\|x - Kx\|^2 + 2^{m-2}\|Kx - T_m Kx\|^2)$$

And by the induction hypothesis $b_m \geq \lambda_m/(2 - \lambda_m)$ and $b_m \geq \sup_{1 \leq i \leq m-1} (\lambda_i/(2 - \lambda_i))$

$$\begin{aligned} \|x - T_n x\|^2 &\leq b_m 2(2^{m-2}\|x - y\|^2 - 2^{m-2}\|Kx - y\|^2 + 2^{m-2}\|Kx - y\|^2 - 2^{m-2}\|Tx - y\|^2) \\ &= b_m 2^{m-1}(\|x - y\|^2 - \|Tx - y\|^2) \end{aligned}$$

And the inequality holds

The fact that T is a reasonable wanderer follows from

$$\begin{aligned} &\sum_{n=0}^{\infty} \|T^n x + T^{n+1} x\| \\ &\leq b_m \cdot 2^{m-1}(\|x - y\|^2 - \|Tx - y\|^2) + b_m \cdot 2^{m-1}(\|Tx - y\|^2 - \|T^2 x - y\|^2) \\ &+ \dots \leq b_m \cdot 2^{m-1} \|x - y\|^2 < \infty \end{aligned}$$

And it follows that T is also asymptotically regular and the sequence $\{T^n x\}$ converges weakly to a fixed point of T . For the theorem to hold true it also needs to be shown that the fixed points of T are points in the intersection of the C_i 's. If x is a point in C_0 , then since $x \in C_i, i = 1 \rightarrow m, x = Tx$. On the other hand if $x = Tx$ and $y \in C_0$,

$$\|x - y\| = \|Tx - Ty\| \leq \|T_1 x - T_1 y\| \leq \|T_1 x - y\| \leq \|x - y\|$$

Which is only possible if $x = T_1 x$ so that $x = T_m \dots T_2 x$, a repetition of the argument leads to $x \in C_i, i = 1 \rightarrow m$ therefore $x \in C_0$

And $x = T_m \dots T_3 x$, therefore $x \in C_i$ for all i and it follows that $x \in C_0$, which completes the proof.

6. Finding projection operators

The iterative procedure described above relies on projection operators that consecutively project an initial point onto a number of convex sets. In a SR context, the convex sets are based on a priori information of the specific situation. Theorem 5.1 gives the foundation for how projection operators onto the respective sets are derived, the theorem describes projection operators to be the result of solving a constrained minimization problem. In order to find an analytical expression for the projection one can often rely on Karush-Kuhn-Tucker (KKT) conditions and in some cases also derive

the projection by logical reasoning. A number useful convex sets to use when implementing POCS can be found in [3] and a selection of sets are given below.

Variance of the residual

Looking at the linear model one notice that the information needed to restore the original signal is information on the point spread function and the statistical properties of the noise process. A constraint based on the variance of the residual can be constructed if one assumes the residual to be approximately equal to the variance of the noise. This constraint is formulated as follows

$$C_v = \{f \mid \|g - Hf\|^2 \leq \epsilon\}$$

The POCS method states that the constraints are to be closed and convex. The set C_v is convex since if f_1 and f_2 are two points in C_v then $f_3 = \alpha f_1 + (1 - \alpha)f_2$ is also contained in C_v , since

$$\|g - Hf_3\| = \|g - H(\alpha f_1 + (1 - \alpha)f_2)\|$$

$$\|g - Hf_3\| = \|\alpha(g - Hf_1) - (1 - \alpha)(g - Hf_2)\|$$

$$\|g - Hf_3\| \leq \|\alpha(g - Hf_1)\| + \|(1 - \alpha)(g - Hf_2)\|$$

$$\|g - Hf_3\| \leq \sqrt{\epsilon}$$

The projection on C_v is found by

$$\min \|f - f_p\|^2$$

$$s. t \ \|g - Hf_p\|^2 = \epsilon$$

In this case the projection operator on C_v will be found with KKT.

$$L(f_p, \lambda) = f_p^T f_p - f_p^T f + f^T f + \lambda(g^T g - 2g^T Hf_p + f_p^T H^T Hf_p - \epsilon)$$

$$L_{f_p}(f_p, \lambda) = 0$$

$$f_p - f - \lambda g^T H + \lambda H^T Hf_p + \lambda H^T Hf - \lambda H^T Hf = 0$$

$$\left(H^T H + \frac{1}{\lambda}\right) f_p = \left(H^T H + \frac{1}{\lambda}\right) f + H^T (g - Hf)$$

$$f_p = f + \left(H^T H + \frac{1}{\lambda} I\right)^{-1} H^T (g - Hf)$$

The multiplier λ can be found by substitution into the equation

$$(g - Hf_p)^t (g - Hf_p) = \epsilon$$

Substituting the above expression and setting $Y = \left(H^t H + \frac{1}{\lambda} I\right)^{-1}$ gives

$$f_p = f + YH^t (g - Hf)$$

and

$$\begin{aligned} (g - Hf_p)^t (g - Hf_p) &= (g - Hf)^t \left(I - HY \quad H^t - HY \quad H^t + H(Y)^t H^t HY \quad H^t \right) (g - Hf) \\ &= (g - Hf)^t \left(I - HY \quad H^t - HYH^t \left(H^t H + \frac{1}{\lambda} I \right) Y \quad + H(Y)^t H^t HY \quad H^t \right) (g - Hf) \\ &= (g - Hf)^t \left(I - HYH^t - \frac{1}{\lambda} IHY^2 H^t - H(Y)^t H^t HYH^t + H(Y)^t H^t HYH^t \right) (g - Hf) \\ &= (g - Hf)^t \left(I - HYH^t - \frac{1}{\lambda} IHY^2 H^t \right) (g - Hf) \end{aligned}$$

The projection on C_v now relies on finding λ . In the case where the image has been degraded by LSI blur the matrix H is circulant and λ can be found by utilizing Plancharels formula

$$\begin{aligned} \|g - Hf\|^2 &= \langle g - Hf, g - Hf \rangle = \left\langle \left(\frac{1}{N} \sum_{n=0}^{N-1} (\widehat{g - Hf}) e^{j2\pi nk/N} \right), \left(\frac{1}{N} \sum_{n=0}^{N-1} (\widehat{g - Hf}) e^{j2\pi mk/N} \right) \right\rangle \\ &= \frac{1}{N^2} \sum_{n=0}^{N-1} \sum_{m=0}^{N-1} \langle (\widehat{g - Hf}) e_n \rangle \langle (\widehat{g - Hf}) e_m \rangle = \frac{1}{N^2} \sum_{n=0}^{N-1} \sum_{m=0}^{N-1} (\widehat{g - Hf})_n (\widehat{g - Hf})_m \langle e_n \rangle \langle e_m \rangle \\ &= \frac{1}{N^2} \sum_{n=0}^{N-1} (\widehat{g - Hf})_n (\widehat{g - Hf})_n N = \frac{1}{N} \sum_{n=0}^{N-1} \|\widehat{g - Hf}\|^2 \\ &= \frac{1}{N} \sum_{n=0}^{N-1} \|\widehat{g - Hf}\|^2 \\ &= \frac{1}{N} \sum_{n=0}^{N-1} (g(k) - H(k)f(k)) \left(I - H(k)H(k) \left(H(k)H(k) + \frac{1}{\lambda} \right) \right. \\ &\quad \left. - \frac{1}{\lambda} H(k)H(k) \left(H(k)H(k) + \frac{1}{\lambda} \right)^2 \right) (g(k) - H(k)f(k)) \\ &= \frac{1}{N} \sum_{n=0}^{N-1} |g(k) - H(k)f(k)|^2 \frac{1}{(\lambda|H(k)|^2 + 1)^2} \end{aligned}$$

λ can now be found by minimizing the above expression.

$$\frac{\partial}{\partial \lambda} \|g - Hf\|^2 = \frac{1}{N} \sum_{n=0}^{N-1} \frac{|g(k) - H(k)f(k)|^2 |H(k)|^2}{(|H(k)|^2 + \frac{1}{\lambda})^3}$$

Outlier of the residual

The set associated with extreme values of the residual is based on the probability distribution of the noise. A common case is to assume that the noise process is Gaussian. With the assumption of Gaussian noise one can find confidence limits from tables. The convex set is given by

$$C_0 = \{f \mid |g_i - [Hf]_i| \leq \epsilon_0\}$$

Convexity of C_0 can be shown by taking two points f_1 and f_2 in C_0 by letting $f_3 = \alpha f_1 + (1 - \alpha)f_2$, it follows that $f_3 \in C_0$

$$|g - [Hf_3]_i| = |g - [H(\alpha f_1 + (1 - \alpha)f_2)]_i|$$

$$|g - [Hf_3]_i| = |\alpha(g - [Hf_1]_i) - (1 - \alpha)(g - [Hf_2]_i)|$$

$$|g - [Hf_3]_i| \leq \alpha \|g - [Hf_1]_i\| + (1 - \alpha) \|g - [Hf_2]_i\| \leq \epsilon_0$$

The projection on C_0 is found from the solution of

$$\min \|f_p - f\|^2$$

$$s. t \mid g_i - [Hf_p]_i \mid \leq \epsilon_0$$

The solution can be found by using the KKT conditions, for $g_i - [Hf_p]_i > 0$

$$L(f_p, \lambda) = f_p^T f_p - f_p^T f + f^T f + \lambda (g_i - [Hf_p]_i)$$

$$L_{f_p}(f_p, \lambda) = 2f_p - 2f - \lambda h_i$$

$$L_{f_p}(f_p, \lambda) = 0$$

$$f_p = \frac{2f - \lambda h_i}{2}$$

And the associated projection is given by

$$f_p = \begin{cases} f + \left(\frac{g_i - h_i f - \epsilon_0}{\|h_i\|^2} \right) h_i & g_i - h_i f > \epsilon_0 \\ f + \left(\frac{g_i - h_i f + \epsilon_0}{\|h_i\|^2} \right) h_i & g_i - h_i f < -\epsilon_0 \end{cases}$$

Mean of the residual

This set is based on the assumption that the noise is zero mean, the convex set is defines as

$$C_m = \left\{ f \mid \left| \sum_{i=1}^N g_i - [Hf]_i \right| \leq \epsilon_m \right\}$$

The bound ϵ_m represents confidence limits on the sample mean.

The projection on C_m is given by

$$f_p = \begin{cases} f + \left(\frac{\sum r_i - \epsilon_m}{\|h_c\|^2} \right) h_c & \sum r_i > \epsilon_m \\ f + \left(\frac{\sum r_i + \epsilon_m}{\|h_c\|^2} \right) h_c & \sum r_i < -\epsilon_m \end{cases}$$

7. Image enhancement

Image super resolution is closely connected to single image restoration theory. Image super resolution can be seen as a second generation image restoration problem and the main principles of single image restoration are valid in a super resolution setting. Thus the various known results to restore one image by POCS can be generalized to the new problem of restoring one single image from a sequence of degraded versions. The main difference between single image restoration and image super resolution is that image super resolution aims at improving the sharpness in an image by recovering high frequency components that are lost due to under sampling the image signal. The sections below illustrate the use of POCS in both single image restoration and in super resolution through an experiment.

7.1. Single image restoration by POCS

In the following experiment a monochrome $[100 \times 100]$ pixel image of a flower is used. The degraded and noisy images are obtained by blurring the original image with a linear PSF and also adding Gaussian white noise at 20 and 10 dB blurred signal to noise ratio respectively.

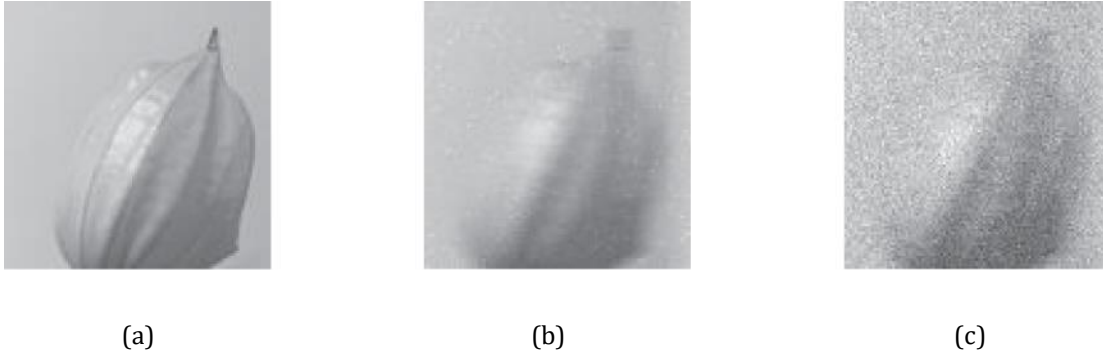


figure 6: (a) original image, (b) 10 db blur, (c) 20 db blur.

One aim of this first experiment is to illustrate the mechanics of POCS in a setting where only one image is used in the restoration procedure before proceeding to solve the image super resolution problem. Another aim is to investigate the effect of noise on a solution that can be deemed to be feasible. A feasible solution in this case refers to a solution that satisfies all defined constraints. Since the constraints are implemented as convex sets the solution is found in the intersection of these sets. In this experiment two sets are used, one set representing the variance of the noise and one set representing outlier of the noise. Noise is only one of the factors that influence the solution, the PSF and the initial estimate of f , used to start the iteration process, are also important factors to consider. When examining how the POCS improves the observed image, MSE between the observed image and the final estimate is used.

The ideal image, the observed image and the final estimate for the 10 db case are shown below.

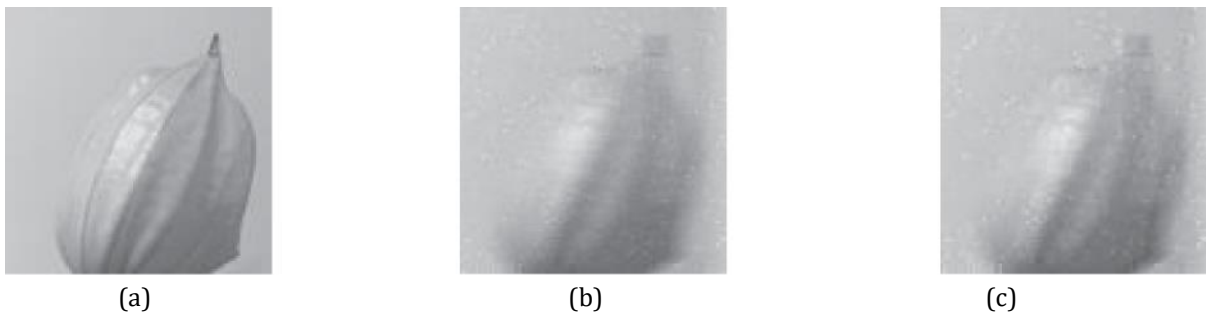


figure 7: (a) original image, (b) observed image, (c) final projection.

A visual inspection of the above images results in the conclusion that the improvement of the iteration procedure gives very small improvements. The visual improvements are slightly more defined edge along the plants center part.

The same images for the increased level of noise is found below.

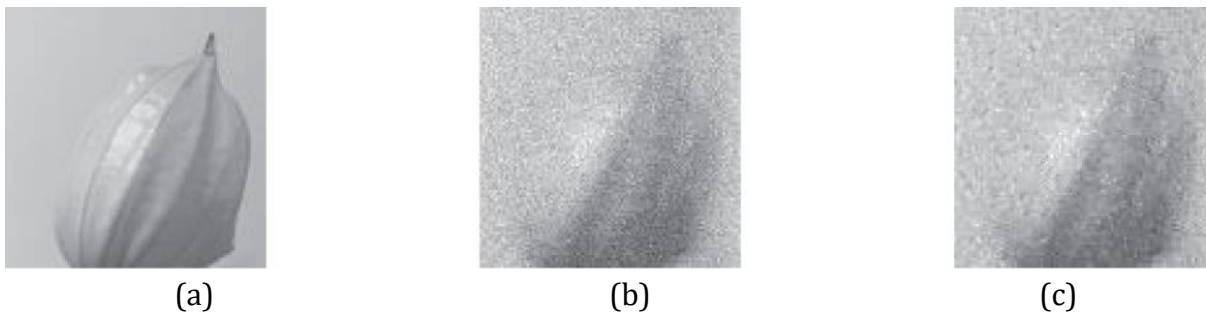


figure 8: original image, (b) observed image, (c) final projection.

Visual inspection of the above images results in the same conclusion as the previous case where a lower level of noise was used, there is a slight improvement between the observed and final estimate. The largest impact on the difference between the observed and final estimate stems from the initial estimate that is used to start the iterative procedure.

In order to give a more precise description of the difference between the ideal image and the result of the POCS procedure the MSE for the different images the given in the table below.

Noise level/Iteration step	Observed image	Final iteration
20 db image	0,0066	0,0048
10 db image	0,0038	0,0027

The table above confirms the conclusion drawn from visual inspection, the improvements in MSE for the respective iterations is small. This result is in line with what can be expected from the POCS algorithm. Each projection onto the respective sets used in the restoration procedure results in a new estimate that in some sense is the closest point to the previous estimate. As a result the deviation from the initial estimate can be small, this result becomes obvious when studying the updating procedure that follows with the different convex sets. In order for the POCS procedure to produce a reasonable estimate of the ideal image much effort is needed to create a high quality starting point for the iterative procedure. If a smooth final estimate is desired a smooth initial estimate is required. In the above example the initial estimate was created by applying a Gaussian filter to the observed image. From the above analysis one can draw the conclusion that the solution set increases with the size of noise, that is, as the variance increases, so does the size of the set where a solution is found. As the noise increases, the quality of the restored signal decreases and since the number of feasible solutions gets larger, it is harder to find final version with high quality.

7.2. Image super resolution by POCS

Image super resolution with POCS is based on the same theory as the single image experiment above. The main difference in the restoration procedure between the two situations is the available information. In the case of super resolution a sequence of degraded versions of the ideal signal is used in the POCS procedure. The restoration procedure is based on the following model that was introduced in section 3.1.

$$g_k = D_k C_k F_k f_k + \varepsilon_k \text{ for } 1 \leq k \leq N$$

In equation above F_k is a $[L^2 \times L^2]$ matrix representing the geometric warp on f , C_k is a linear space variant blur matrix of size $[L^2 \times L^2]$ and D_k is a $[M_k^2 \times L^2]$ matrix representing the decimation on f_k . The following experiment consists of super resolution reconstruction with two different sets of observations. The first set consists of four images of size $[50 \times 50]$ and the second set consist of 16 images of the same size. The two different sets will be used to investigate how a larger number of images will affect

the final estimate of the ideal signal. All degraded images were created by randomly displacing pixels uniformly over an interval of 0 to five pixels. Each of the displaced versions of the ideal image were the degraded by linear motion blur with two different levels of Gaussian noise and also decimated by a factor of 0.5.

The ideal image and the degraded versions for the 16 image case is shown below.

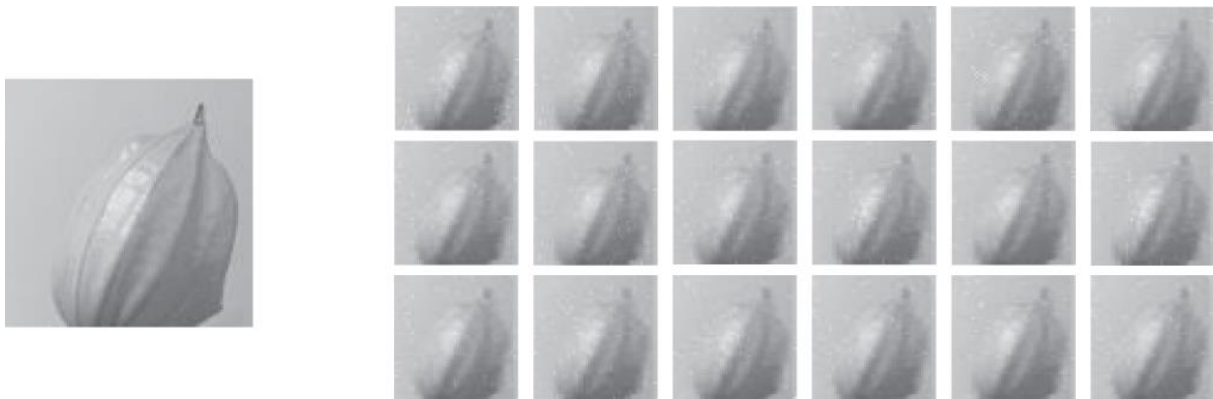


figure 9: Original and the simulated observed versions.

The aim of the super resolution procedure is to use the subpixel differences in the down sampled images together with a priori information on the solution to create an estimate of the ideal image. The same convex sets that were used in previous section will be used in the POCS procedure for each of the down sampled versions. Each individual image for both cases where treated with POCS and the pixels for each individual image were superimposed on a grid representing the pixel density of the ideal signal, in this case a $[100 \times 100]$ grid.

An illustration of the procedure is shown below.

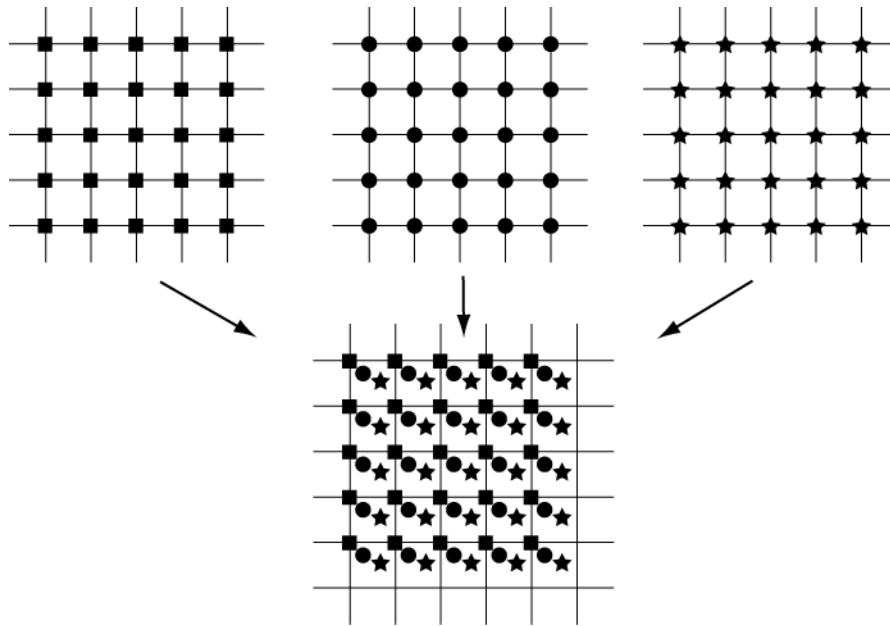


figure 10: Technique for merging the observed low resolution images on a high resolution grid

In the illustration above three images are merged into a final SR image. The creation of the final estimate of the ideal image in this experiment is created in a similar way. In the first case four restored images are merged into the final estimate and in the second case 16 images are used. The result of the procedure is shown below.

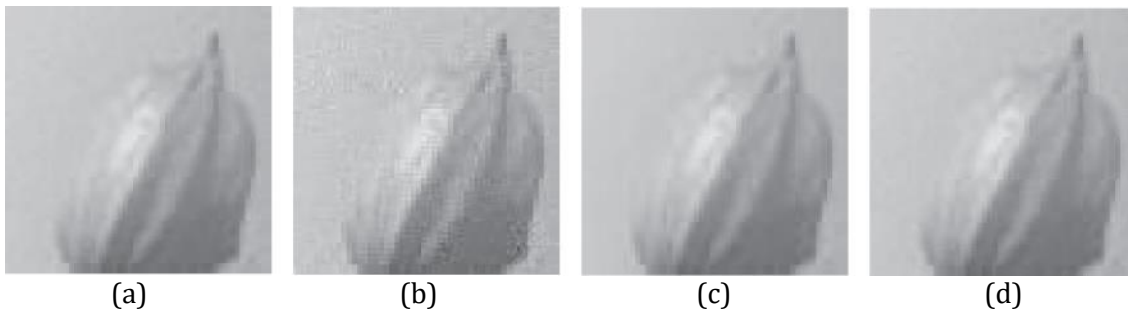


figure 11: (a) Four image reconstruction with 0.005 noise level, (b) four image reconstruction with 0.05 noise level, (c) sixteen image reconstruction with 0.005 noise level, (d) sixteen image reconstruction with 0.05 noise level

Visual inspection of the final estimates shows that a larger number of images used in the restoration decreases the impact of noise.

A more detailed description of the difference between the ideal image and the respective SR images can be found by calculating the MSE for the different cases, MSE for the different cases is given in the table below.

<i>Noise level/Images used in restoration</i>	<i>4 images</i>	<i>16 images</i>
<i>0.05 noise level</i>	0.001	0.0005
<i>0.005 noise level</i>	0.001	0.0004

The above table confirms the result of the visual inspection. A larger number of images improves the final estimate. As in the case of single image restoration the initial estimate and the level of noise are the main drivers of the final result. The effect of noise decreases when a larger number of images are available. When analyzing the above result a natural question is if it is possible to improve the procedure above by taking the number of images available and the noise level into account. A Tikhonov approach to restoration procedure makes this possible.

8. Discussion and results

The POCS approach to super resolution is one of several methods available to increase the resolution in images. Increasing the resolution by restoring high frequency components in the original signal that are lost during sampling is the primary goal of super resolution. Most work on POCS can be traced back to articles written during the 80's and 90's. Even though super resolution is an interesting area it seems as there are other approaches that can be more successful in real world applications. The results in this paper gives insight to some of the difficulties with the POCS approach. One of the most obvious results is the dependency between the final result and the initial estimate. By analyzing the iterative updating procedure used when applying POCS this becomes both clear and it's also intuitive. Each projection onto the respective sets used in the restoration procedure results in a new estimate that in some sense is the closest point to the previous estimate. As a result the deviation from the initial estimate can be small, this result is in line with the simulation made in this paper. Another feature of the solution is that it's not unique. The final estimate depends on the initial estimate but also on the order of the projections, by interchanging the projection order a different final estimate will be found. There is one exception to this rule and this is the case where all sets used by defining the solution set are linear varieties [13]. When all sets are linear varieties the final estimate is the orthogonal projection of the final estimate onto the intersection of all defined sets. There are options available to overcome the weakness of a nonunique final estimate. One alternative is described in [14] where the authors extend the POCS method by implementing hybrid between maximum likelihood and POCS it is also shown that this approach results in a unique solution to the problem. A problem related to the problem of nonuniqueness is the size of the solution set. A larger set of feasible solutions results in greater variation. The size of the solution set depends on how the convex sets are defined and in the experiment in this paper the solution set depends on the size of the noise. Another related problem is if there is an

intersection between the defined sets. From the presented experiment it becomes clear that knowledge about the PSF is needed when applying POCS. In a real world situation the PSF is unknown and needs to be estimated. There are several techniques for estimating PSF:s described in the literature and knowledge about the PSF is an important condition when implementing the procedure. The complexity of super resolution problem increases with the complexity of the PSF. More complex PSF examples arise in situation where blur varies within the registered image. This type of blur is referred to as space varying blur and there are examples where space varying blur has been modeled with POCS [9]. When space varying blur is modeled one needs to specify the convex sets in accordance with the blur region. Since POCS can model convex sets on a pixel level the POCS technique is well suited to model this type of blur. Another feature of super resolution image reconstruction is registration of the observed images onto a grid representing the target resolution. This is usually done by choosing one of the observed images as a starting point and finding common point to use as reference when merging new images onto the super resolution grid. In the above experiment the first image was chosen arbitrary and the following images were registered without no specific order. This solution is somewhat simplified compared to what would have to be done in a real world situation. Most work in this paper has been devoted to writing Matlab code to implement the presented theory. The results shown are a minor part of the tests that has been made with trying to find workable procedure to implement POCS. The first attempts to implement the procedure were based on a [500x500] image. This size is in no aspect very large, even so, implementing the convex set defined by the variance of the noise showed to be impossible with the computer power available. To mitigate the problem one attempt was to divide the [500x500] image in parts of [50x50] and treat the parts independently and as a last step merge the different parts together. This approach resulted in a final estimate where blocks where optimized independent and edges became visible between the different parts in the final result. This problem points out another problem with the procedure, it's very compute intense. Overall the mathematics behind the POCS procedure is interesting and the purpose of the technique has nice connection to the well-known problem of increasing resolution in images. Even though the theory is interesting and there are many applications the results presented here indicate that there are a lot of steps to work through and consider in order for the procedure to be result in a reasonable final estimate of the ideal image.

Appendix A

Proof of theorem 5.6. For every $y \in \mathfrak{S}$, the sequence $\{d_n\} = \{\|T^n x - y\|\}$ is nonincreasing since

$$d_{n+1} = \|T^{n+1}x - y\| = \|T(T^n x) - Ty\| \leq \|T^n x - y\| = d_n$$

Therefore the nonnegative limit

$$d(y) = \lim_{n \rightarrow \infty} \|T^n x - y\|$$

Exists for every $y \in \mathfrak{S}$. According to lemma 5.1, \mathfrak{S} is a closed convex subset of C and it follows that for any fixed $\delta \geq 0$, the set

$$\mathfrak{S}_\delta = \{y \in \mathfrak{S}: d(y) \leq \delta\}$$

Is a closed and bounded convex subset of \mathfrak{S} which is nonempty for δ large enough. Convexity and closure follows from $d(y) = \lim_{n \rightarrow \infty} \|T^n x - y\|$

and boundedness is implied by

$$\|y\| = \|y - T^n x + T^n x\| \leq \|T^n x - y\| + \|T^n x\|$$

and

$$\|T^n x\| = \|T^n x - y_0 + y_0\| \leq \|T^n x - y_0\| + \|y_0\|$$

Bounded closed convex sets are weakly compact, therefore the intersection of these sets is a closed bounded set \mathfrak{S}_{δ_0} . The set \mathfrak{S}_{δ_0} can contain only one element, let y_0 represent this element. If we suppose that \mathfrak{S}_{δ_0} also contains $y_1 \neq y_0$ the identity

$$\left\| T^n x - \frac{y_0 + y_1}{2} \right\| = \frac{1}{2} (\|T^n x - y_0\|^2 + \|T^n x - y_1\|^2) - \left\| \frac{y_0 + y_1}{2} \right\|^2$$

Gives $d[(y_0 + y_1)/2]$, which contradicts the meaning of δ_0 . To prove that $T^n x$ converges to y_0 it needs to be shown that that all possible weak limits of its various subsequences is equal to y_0 . Let $T^{n'} x \rightarrow y_1 \neq y_0$. From the asymptotic regularity of T

$$T^{n'} x - T^{n'+1} x = (1 - T)T^{n'} x \rightarrow \phi$$

By demiclosedness of $(1 - T)$, $(1 - T)y_1 = \phi$, which gives that y_1 is a fixed point of T , by lemma 2.2

$$\delta_0 = \lim \|T^n x - y_0\| > \lim \|T^{n'} x - y_1\| = d(y_1)$$

A result that is incompatible with the meaning of δ_0 .

Appendix B

Processing steps

%Create down sampled images with noise

```
[A B]=Down('Uppsats100x100.jpg',0.05);
```

```
[C D]=Down('Uppsats100x100.jpg',0.01);
```

%Calculate MSE between the images created in the previous stage
%and the ideal image

```
MSE1=MSE('Uppsats100x100.jpg', 'fDownBrus0.05.jpg');
```

```
MSE1=MSE('Uppsats100x100.jpg', 'fDownBrus0.01.jpg');
```

```
MSE1=MSE('Uppsats100x100.jpg', 'fInitial0.05.jpg');
```

```
MSE1=MSE('Uppsats100x100.jpg', 'fInitial0.01.jpg');
```

%Create a first estimate of the ideal image with the first POCS iteration

```
x=POCS1('fDownBrus0.05.jpg','fInitial0.05.jpg',0.05,1);
```

```
x=POCS1('fDownBrus0.01.jpg','fInitial0.01.jpg',0.01,1);
```

% Calculate MSE between the previous estimate and the ideal image

```
MSE1=MSE('Uppsats100x100.jpg', 'fDownBrusPocs10.05.jpg');
```

```
MSE1=MSE('Uppsats100x100.jpg', 'fDownBrusPocs10.01.jpg');
```

%Calculate lambda

```
x=POCS2Lambda()
```

%Create a second estimate of the ideal image

```
x=POCS2('fInitial0.01.jpg','fDownBrusPocs10.01.jpg',0.01,0.2);
```

```
x=POCS2('fInitial0.05.jpg','fDownBrusPocs10.05.jpg',0.05,0.2);
```

% Calculate MSE between the previous estimate and the ideal image

```
MSE1=MSE('Uppsats100x100.jpg', 'fDownBrusPocs20.010.2.jpg');
```

```
MSE1=MSE('Uppsats100x100.jpg', 'fDownBrusPocs20.050.2.jpg');
```

%Create SR images with POCS

%Create images with subpixel differences

```
x=SRbilder('Uppsats100x100.jpg',4)
```

%Create resized images

```
f=imread('SRdelBild1.jpg');
```

```
f = imresize(f,0.5);
```

```
imwrite(f,'SRdelBild1x0.5.jpg');
```

```
f=imread('SRdelBild2.jpg');
```

```

f = imresize(f,0.5);
imwrite(f,'SRdelBild2x0.5.jpg');

f=imread('SRdelBild3.jpg');
f = imresize(f,0.5);
imwrite(f,'SRdelBild3x0.5.jpg');

f=imread('SRdelBild4.jpg');
f = imresize(f,0.5);
imwrite(f,'SRdelBild4x0.5.jpg');

f=imread('Uppsats100x100.jpg');
f = imresize(f,0.5);
imwrite(f,'SRinitialx0.5.jpg');

%Add motionblur and noise
[A B]=DownSR('SRdelBild1.jpg',0.005);
[A B]=DownSR('SRdelBild2.jpg',0.005);
[A B]=DownSR('SRdelBild3.jpg',0.005);
[A B]=DownSR('SRdelBild4.jpg',0.005);

%Run the POCS procedure
x=POCS1SR('fDownSRBrus10.005.jpg','SRinitialx0.5.jpg',0.005,1);
x=POCS1SR('fDownSRBrus20.005.jpg','SRinitialx0.5.jpg',0.005,1);
x=POCS1SR('fDownSRBrus30.005.jpg','SRinitialx0.5.jpg',0.005,1);
x=POCS1SR('fDownSRBrus40.005.jpg','SRinitialx0.5.jpg',0.005,1);

%Merge images for the lowest noise level to create a SR image
x=concatSR1();
imwrite(x,'SRUppsats100x100x4x0.005.jpg');

%Repeat the procedure with 16 images
x=SRbilder('Uppsats100x100.jpg',16);

%Downsample images
x=nerSamplaSRdel(16);

%Add motionblur and noise
[A B]=DownSR1(0.005)

%Run the POCS procedure
x=POCS1SR1('SRinitialx0.5.jpg',0.005,1);

%Merge the images to create an estimate of the ideal image
x=concatSR2(0.005);
a=imresize(x,0.5,'bilinear');
imwrite(a,'SRUppsats100x100x16x0.005.jpg');

%Repeat the procedure with increased level of noise
[A B]=DownSR1(0.05);

```

```

%Run the POCS procedure
x=POCS1SR1('SRinitialx0.5.jpg',0.05,1);

%Merge images to create an estimate of the ideal image
x=concatSR2(0.05);
a=imresize(x,0.5,'bilinear');
imwrite(a,'SRUppsats100x100x16x0.05.jpg');

%Använd de fyra första bilderna av brusnivån 0.05 för att skapa en SR bild
x=concatSR1();
imwrite(x,'SRUppsats100x100x4x0.05.jpg');

%Calculate MSE
MSE1=MSE('Uppsats100x100.jpg', 'SRUppsats100x100x4x0.005.jpg');
MSE1=MSE('Uppsats100x100.jpg', 'SRUppsats100x100x4x0.05.jpg');
MSE1=MSE('Uppsats100x100.jpg', 'SRUppsats100x100x16x0.005.jpg');
MSE1=MSE('Uppsats100x100.jpg', 'SRUppsats100x100x16x0.05.jpg');

```

Down.m

```

%Create downsampled images with motionblur and noise
function [A B]=Down(n,brus)
forg=imread(n);
forg=im2double(forg);
forg=reshape(forg,[],1);
H=fspecial('motion',10,180);
H=[H, zeros(1,9989)];
c = [H(1) fliplr(H(end-length(H)+2:end))];
r=H;
conv=toeplitz(c,r);
fdown=conv*forg;
fdown=vec2mat(fdown,100);
imwrite(fdown,'fDownx100x100.jpg');
fDownBrus=conv*forg+normrnd(0,brus,10000,1);
for i=1:1:10000
    rect=rand;
    if rect<0.02
        fDownBrus(i)=fDownBrus(i)+0.1;
    end;
end;

fDownBrus=vec2mat(fDownBrus,100);
brusString=num2str(brus);
bildNamn=strcat('fDownBrus',brusString);
bildNamn=strcat(bildNamn,'.jpg');
imwrite(fDownBrus,bildNamn);
fInitial = imgaussfilt(fDownBrus);
brusString=num2str(brus);
bildNamn=strcat('fInitial',brusString);
bildNamn=strcat(bildNamn,'.jpg');
imwrite(fInitial,bildNamn);

```

```
A=fDownBrus;
B=fdown;
```

MSE.m

```
function Mean_Square_Error= MSE(Reference_Image, Target_Image)
Reference_Image=imread(Reference_Image);
Target_Image=imread(Target_Image);
Reference_Image = im2double(Reference_Image);
Target_Image = im2double(Target_Image);
[M N] = size(Reference_Image);
error = Reference_Image - Target_Image;
Mean_Square_Error = sum(sum(error .* error)) / (M * N);
end
```

POCS1.m

```
function x=POCS1(obsBild,start,brus,antallter)
fdownbrus=imread(obsBild);
fdownbrus=im2double(fdownbrus);
fstart=imread(start);
fstart=im2double(fstart);
fdownbrus=reshape(fdownbrus.',[],1);
fstart=reshape(fstart.',[],1);
nollV=zeros(1,10000);
fpocs1=zeros(1,10000);
H=fspecial('motion',5,180);
H=[H, zeros(1,9995)];
c = [H(1) fliplr(H(end-length(H)+2:end))];
r=H;
conv=toeplitz(c,r);
h=fspecial('motion',5,180);
res=fdownbrus-conv*fstart;
for j=1:1:antallter
    for i=1:1:10000
        ri=res(i);
        if i<9995
            positions=[i:4+i];
            convVector=nollV;
            convVector(positions)=h;
            convVector=transpose(convVector);
        end
        if (ri)>brus
            a=fstart+(1/((norm(h)^2)))*(ri-brus)*convVector;
        elseif (ri)<-brus
            a=fstart+(1/((norm(h)^2)))*(ri+brus)*convVector;
        else
            a=fstart;
        end;
        fpocs1(i)=a(i);
        clear a;
    end
end
```

```

end;
fdownbrus=fstart;
fstart=fpocs1;
end;
fpocs1=vec2mat(fpocs1,100);
brusString=num2str(brus);
bildNamn=strcat('fDownBrusPocs1',brusString);
bildNamn=strcat(bildNamn,'.jpg');
imwrite(fpocs1,bildNamn);
x=fpocs1;

```

POCS2.m

```

function x=POCS2(obsBild,start,brus,lambda)
fstart=imread(obsBild);
fstart=im2double(fstart);
fstart=reshape(fstart,[],1);
fpocs1=imread(start);
fpocs1=im2double(fpocs1);
fpocs1=reshape(fpocs1,[],1);
H=fspecial('motion',5,180);
H=[H, zeros(1,9995)];
c = [H(1) fliplr(H(end-length(H)+2:end))];
r=H;
conv=toeplitz(c,r);
res=fpocs1-conv*fstart;
fpocs2=fpocs1+inv(transpose(conv)*conv+((1/lambda))*eye(10000))*transpose(conv)*res;
fpocs2=vec2mat(fpocs2,100);
brusString=num2str(brus);
lambdaString=num2str(lambda);
bildNamn=strcat('fDownBrusPocs2',brusString);
bildNamn=strcat(bildNamn,lambdaString);
bildNamn=strcat(bildNamn,'.jpg');
imwrite(fpocs2,bildNamn);
x=fpocs2;

```

SRbilder.m

```

function x=SRbilder(obsBild,antalBilder)
bild=imread(obsBild);
bild=im2double(bild);
for h=1:1:antalBilder
    for i=1:1:100
        rad=bild(i,:);
        for j=1:5:100
            delRad=rad(j:j+4);
            sortVektor=randperm(5);
            nyDelRad=zeros(1,5);
            for k=1:1:5
                nyDelDelRad=delRad((sortVektor(k)));
            end
        end
    end
end

```

```

        nyDelRad(k)=nyDelDelRad;
    end
    genvarname('A', num2str(j));
    eval(['A' num2str(j) '= nyDelRad']);
end
nyRad=horzcat(A1,A6,A11,A16,A21,A26,A31,A36,A41,A46,A51,A56,A61,A66,A71,A76,A81,
A86,A91,A96);
    genvarname('B', num2str(i));
    eval(['B' num2str(i) '= nyRad']);
end
x=vertcat(B1,B2,B3,B4,B5,B6,B7,B8,B9,B10,B11,B12,B13,B14,B15,B16,B17,B18,B19,B20,B21,B22,
B23,B24,B25,B26,B27,B28,B29,B30,B31,B32,B33,B34,B35,B36,B37,B38,B39,B40,B41,B42,B43,B44,
B45,B46,B47,B48,B49,B50,B51,B52,B53,B54,B55,B56,B57,B58,B59,B60,B61,B62,B63,B64,B65,B66,
B67,B68,B69,B70,B71,B72,B73,B74,B75,B76,B77,B78,B79,B80,B81,B82,B83,B84,B85,B86,B87,B88,
B89,B90,B91,B92,B93,B94,B95,B96,B97,B98,B99,B100);
bildNummer=num2str(h);
utbild=strcat('SRdelBild',bildNummer);
utbild=strcat(utbild,'.jpg');
imwrite(x,utbild);
end;

```

DownSR1.m

```

function [A B]=DownSR1(brus)

for h=1:1:16
    bildNummer=num2str(h);
    bildNamn=strcat('SRdelBild',bildNummer);
    bildNamn=strcat(bildNamn,'x0.5');
    bildNamn=strcat(bildNamn,'.jpg')
    forg=imread(bildNamn);
    forg=im2double(forg);
    forg=reshape(forg,[],1);

    H=fspecial('motion',3,180);
    H=[H, zeros(1,2497)];
    c = [H(1) fliplr(H(end-length(H)+2:end))];
    r=H;
    conv=toeplitz(c,r);
    fDownBrus=conv*forg+normrnd(0,brus,2500,1);
    for i=1:1:2500
        rect=rand;
        if rect<0.02
            fDownBrus(i)=fDownBrus(i)+0.1;
        end;
    end;

    fDownBrus=vec2mat(fDownBrus,50);
    brusString=num2str(brus);
    bildNamn=strcat('fDownSRBrus',brusString);
    bildNamn=strcat(bildNamn,'x');

```

```

    bildNamn=strcat(bildNamn,bildNummer);
    bildNamn=strcat(bildNamn,'.jpg');
    imwrite(fDownBrus,bildNamn);
    fInitial = imgaussfilt(fDownBrus);
    brusString=num2str(brus);
    bildNamn=strcat('fInitialSR4',brusString);
    bildNamn=strcat(bildNamn,bildNummer);
    bildNamn=strcat(bildNamn,'.jpg');
    imwrite(fInitial,bildNamn);
end;
A=fDownBrus;
B=fInitial;

```

POCS1SR.m

```

function x=POCS1SR(obsBild,start,brus,antallter)
fdownbrus=imread(obsBild);
fdownbrus=im2double(fdownbrus);
fstart=imread(start);
fstart=im2double(fstart);
fdownbrus=reshape(fdownbrus,[],1);
fstart=reshape(fstart,[],1);
nollV=zeros(1,2500);
fpocs1=zeros(1,2500);
H=fspecial('motion',3,180);
H=[H, zeros(1,2497)];
c = [H(1) fliplr(H(end-length(H)+2:end))];
r=H;
conv=toeplitz(c,r);
h=fspecial('motion',3,180);
res=fdownbrus-conv*fstart;
for j=1:1:antallter
    for i=1:1:2500
        ri=res(i);
        if i<2497
            positions=[i:2+i];
            convVector=nollV;
            convVector(positions)=h;
            convVector=transpose(convVector);
        end
        if (ri)>brus
            a=fstart+(1/((norm(h)^2)))*(ri-brus)*convVector;
        elseif (ri)<-brus
            a=fstart+(1/((norm(h)^2)))*(ri+brus)*convVector;
        else
            a=fstart;
        end;
        fpocs1(i)=a(i);
        clear a;
    end;
    fdownbrus=fstart;
end;

```

```

    fstart=fpocs1;
end;
fpocs1=vec2mat(fpocs1,50);
brusString=num2str(brus);
bildNamn=strcat('fDownBrusPocs1SRx4x',brusString);
bildNamn=strcat(bildNamn,'.jpg');
imwrite(fpocs1,bildNamn);

```

ConcatSR2.m

```
function x=concatSR2(brus)
```

```
nyBild=zeros(100);
```

```
nyBild=double(nyBild);
```

```
for h=1:1:16
```

```
    bildNummer=num2str(h);
```

```
    brusString=num2str(brus);
```

```
    bildNamn=strcat('fDownBrusPocs1SRx',bildNummer);
```

```
    bildNamn=strcat(bildNamn,'x');
```

```
    bildNamn=strcat(bildNamn,brusString);
```

```
    bildNamn=strcat(bildNamn,'.jpg');
```

```
    bildi=imread(bildNamn);
```

```
    bildNamn;
```

```
    bildi=im2double(bildi);
```

```
    h;
```

```
if h<5
```

```
    k=h-1;
```

```
    m=0;
```

```
    for i=1:4:197
```

```
        m=m+1;
```

```
        l=0;
```

```
        for j=1:4:197
```

```
            l=l+1;
```

```
            m;
```

```
            l;
```

```
            pixel=bildi(m,l);
```

```
            nyBild(i,j+k)=pixel;
```

```
            i;
```

```
            j;
```

```
        end;
```

```
    end;
```

```
end;
```

```
    if (h > 4) && (h < 9)
```

```
        h
```

```

k=h-5;
m=0;
for i=2:4:198
    m=m+1;
    l=0;
    for j=1:4:197
        l=l+1;
        m;
        l;
        pixel=bildi(m,l);
        nyBild(i,j+k)=pixel;
        i;
        j;
    end;
end;

```

```
end;
```

```
end;
```

```
if (h > 8) && (h < 13)
```

```

k=h-9;
m=0;
for i=3:4:199
    m=m+1;
    l=0;
    for j=1:4:197
        l=l+1;
        m;
        l;
        pixel=bildi(m,l);
        nyBild(i,j+k)=pixel;
        i;
        j;
    end;
end;

```

```
end;
```

```
end;
```

```
if 12<h
```

```

k=h-13;
m=0;
for i=4:4:200
    m=m+1;
    l=0;
    for j=1:4:197
        l=l+1;
        m;
        l;
        pixel=bildi(m,l);

```

```
    nyBild(i,j+k)=pixel;
    i;
    j;
end;

end;

end;

end;
x=nyBild;
```

References

- [1] J. Yang, T. Huang, Image super-resolution: Historical overview and future challenges, CRC press 2010.
- [2] S. C. Park, M. K. Park, M. GiKang, Super-resolution image reconstruction: A technical overview. IEEE Signal processing magazine 2003.
- [3] M. I. Sezan, An overview of convex projection theory and its application to image recovery problems, Ultramicroscopy, Volume 40, Issue 1, January 1992, pages 55-67.
- [4] L.M. Bregman, The relaxation method of finding the common point of convex sets and its solution of problems in convex programming, USSR Computational Mathematics and Mathematical Physics Volume 7, Issue 3, 1967, pages 200-217.
- [5] R. Tsai, T. Huang, Multiframe image registration and restoration, Advances in Computer Vision and Image Processing, Volume 1, 1984, pages 317-339.
- [6] A. M. Tekalp, M. K. Ozkan, M. I. Sezan, High resolution image reconstruction from lower resolution image sequences and space-varying image restoration, IEEE Transactions on Medical Imaging, 1992.
- [7] P. Osukoui-Fard, H. Stark, Tomographic image reconstruction using the theory of convex projections, IEEE Transactions on Medical Imaging, Volume: 7, Issue: 1, Mar 1988.
- [8] P. Osukoui-Fard, H. Stark, High resolution image recovery from image-plane arrays, using convex projections, IEEE Transactions on Medical Imaging, 1992.
- [9] A. M. Tekalp, M.I. Sezan, POCS - based restoration of space-varying blurred images, IEEE Transactions on Image Processing, Volume: 3, Issue: 4, Jul 1994.
- [10] M. I. Sezan, H. J. Trussell, Prototype image constraints for set-theoretic image restoration, IEEE Transactions on Signal Processing, Volume: 39, Issue: 10, Oct 1991.
- [11] A. I. Zayed, Advances in Shannon's sampling theory, Taylor & Francis 1993.
- [12] M. Bazaraa, H. Sherali, C. Shetty, Nonlinear programming theory and algorithms, New York, John Wiley, cop., 2006.
- [13] D. C. Youla, Mathematical theory of image restoration by the method of convex projections, Image recovery theory and application, Academic Press, Inc. 1987.

[14] M. Elad , A. Feuer, Restoration of a single superresolution image from several blurred, noisy, and undersampled measured images, IEEE Transactions on Image Processing, Volume: 6, Issue: 12, Dec 1997.

[15] H. Stark, Image recovery theory and application, Academic Press, 1987.